

# A Robust Real-Time Lane Detection Method with Fog-Enhanced Feature Fusion for Foggy Conditions

Ronghui Zhang<sup>1</sup>, Yuhang Ma<sup>1</sup>, Tengfei Li<sup>1</sup>, Ziyu Lin<sup>1</sup>, Yueying Wu<sup>1</sup>, Junzhou Chen<sup>1</sup>, Lin Zhang<sup>2</sup>, Jia Hu<sup>2</sup>,  
Tony Z. Qiu<sup>3</sup> and Konghui Guo<sup>4</sup>

**Abstract**—Lane detection is a critical component of Advanced Driver Assistance Systems (ADAS). Existing lane detection algorithms generally perform well under favorable weather conditions. However, their performance degrades significantly in adverse conditions, such as fog, which increases the risk of traffic accidents. This challenge is compounded by the lack of specialized datasets and methods designed for foggy environments. To address this, we introduce the FoggyLane dataset, captured in real-world foggy scenarios, and synthesize two additional datasets, FoggyCULane and FoggyTusimple, from existing popular lane detection datasets. Furthermore, we propose a robust Fog-Enhanced Network for lane detection, incorporating a Global Feature Fusion Module (GFFM) to capture global relationships in foggy images, a Kernel Feature Fusion Module (KFFM) to model the structural and positional relationships of lane instances, and a Low-level Edge Enhanced Module (LEEM) to address missing edge details in foggy conditions. Comprehensive experiments demonstrate that our method achieves state-of-the-art performance, with F1-scores of 95.04 on FoggyLane, 79.85 on FoggyCULane, and 96.95 on FoggyTusimple. Additionally, with TensorRT acceleration, the method reaches a processing speed of 38.4 FPS on the NVIDIA Jetson AGX Orin, confirming its real-time capabilities and robustness in foggy environments.

**Index Terms**—ADAS, intelligent vehicle, foggy lane detection dataset, foggy lane detection, global attention, edge enhancement

## I. INTRODUCTION

This work has been submitted to the IEEE for possible publication. Copyright may be transferred without notice, after which this version may no longer be accessible.

This project is jointly supported by National Natural Science Foundation of China (Nos. 52172350, W2421069 and 51775565), the Guangdong Basic and Applied Research Foundation (No. 2022B1515120072), the Guangzhou Science and Technology Plan Project (No. 2024B01W0079), the Nansha Key RD Program (No. 2022ZD014), the Science and Technology Planning Project of Guangdong Province (No. 2023B1212060029). (Corresponding author: Junzhou Chen.)

Ronghui Zhang, Yuhang Ma, Tengfei Li, Ziyu Lin, Yueying Wu and Junzhou Chen are with the Guangdong Key Laboratory of Intelligent Transportation System, School of Intelligent Systems Engineering, Sun Yat-sen University, Guangzhou 510275, China (e-mail: zhangrh25@mail.sysu.edu.cn, mayh39@mail2.sysu.edu.cn, litf23@mail2.sysu.edu.cn, linzy88@mail2.sysu.edu.cn, wuyy236@mail2.sysu.edu.cn, chenjunzhou@mail.sysu.edu.cn).

Lin Zhang is with the College of Automotive Studies, Tongji University, Shanghai 201804, China (e-mail: tongjizl@tongji.edu.cn).

Jia Hu is with the College of Transportation Engineering, Tongji University, Shanghai 201804, China (e-mail: hujia@tongji.edu.cn).

Tony Z. Qiu is with Department of Civil and Environmental Engineering, University of Alberta, Edmonton, Alberta, Canada (e-mail: zhijun-qiu@ualberta.ca).

Konghui Guo is with the State Key Laboratory of Automotive Chassis Integration and Bionics, Jilin University, Changchun 130025, China (e-mail: guokh@jlu.edu.cn).

**L**ANE detection plays an important role in Advanced Driver Assistance Systems (ADAS), providing essential support for lane keeping, autonomous navigation, and lane departure warnings, which help reduce the risk of lane-deviation accidents. As intelligent driving technologies advance, the need for robust and real-time lane detection in complex road environments is becoming more apparent, making it a key research focus in autonomous driving [1].

Under good weather and clear lane markings, current lane detection algorithms perform well. However, in complex road environments and poor weather, such as fog, lane markings can become blurred, image quality may decrease, and global environmental information is often obscured, which makes lane detection more challenging. In these conditions, existing algorithms often struggle and may fail, leading to an increased risk of traffic accidents with more severe consequences. Ensuring safe driving in these conditions calls for the development of high-precision, highly robust lane detection methods optimized for foggy environments. As shown in Fig. 1, the in-vehicle camera captures real-time road images, which are preprocessed by edge devices and then sent to the lane detection module. Detected lane information is fused with data from other sensors, such as radar and GPS, along with real-time traffic data from the cloud. This information is processed in the vehicle's computing unit, allowing the system to make adaptive driving decisions—such as accelerating, braking, or steering—to ensure safety in challenging environments like fog.

Earlier lane detection algorithms mainly relied on traditional computer vision methods, involving image preprocessing, feature extraction, and lane model fitting. Son et al. [3] first detected the vanishing point to select the ROI adaptively, then extracted lane markings based on color features and performed clustering. Hou et al. [4] used the Canny operator for edge detection and applied a progressive probabilistic Hough transform to detect lines. While these feature-based methods are efficient and suitable for real-time applications, they require manual parameter tuning and struggle in challenging conditions such as worn or occluded lane markings.

With deep learning's success in image tasks, it has become the mainstream approach for lane detection due to its strong feature extraction capabilities and better generalization. Deep learning offers higher robustness, adapting well to complex road environments and handling missing or occluded lane markings [5]–[10]. However, many networks rely on pixel-by-pixel classification, whereas lane detection does not require

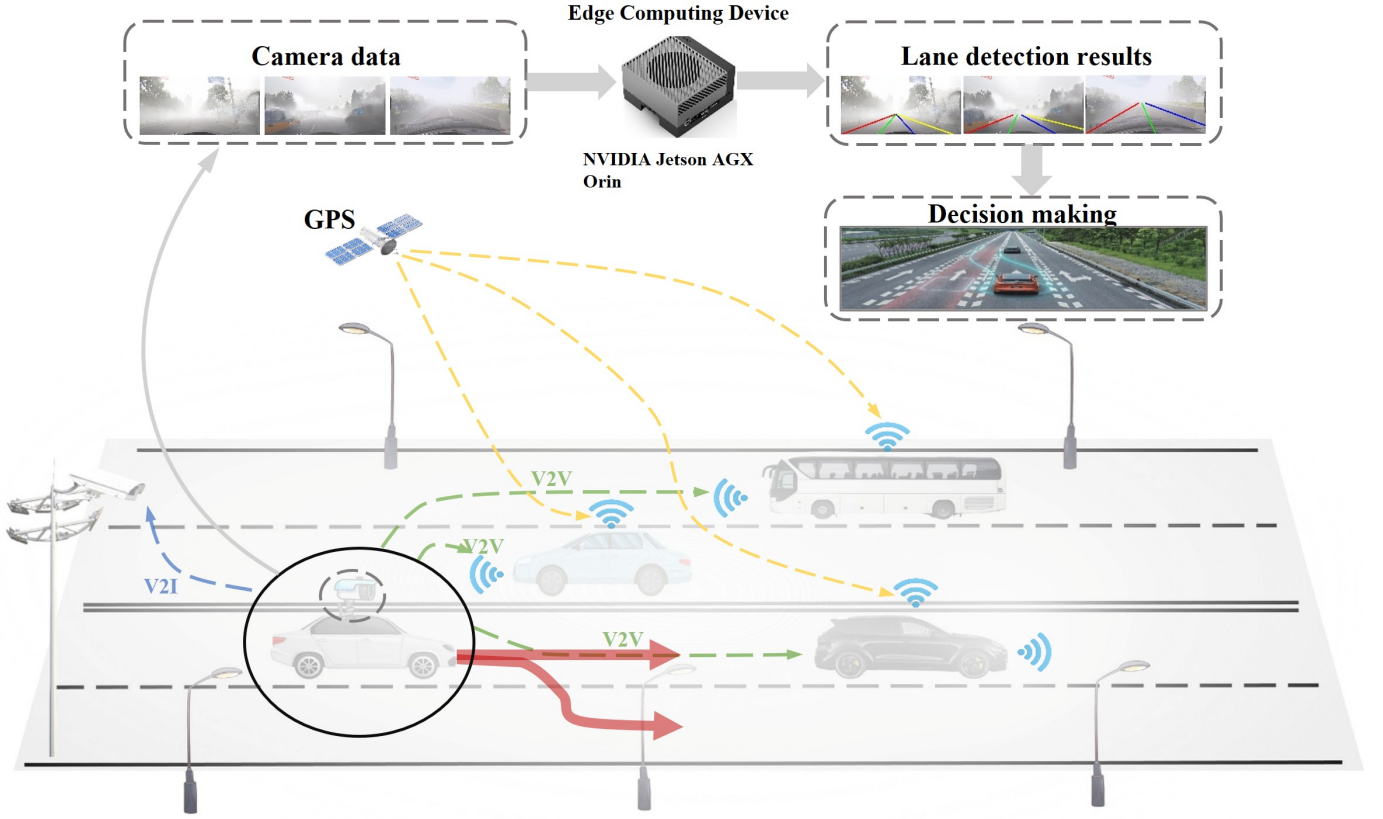


Fig. 1. Lane detection in foggy scenarios for ADAS. [2]

dense pixel segmentation. Qin et al. [11] addressed this by re-framing lane detection as a row-based segmentation problem, reducing computational cost and improving detection speed.

In addition to segmentation methods, lane detection also includes detection-based approaches, many borrowing Anchor-based methods from object detection [12]–[15]. Due to the elongated shape of lane lines, traditional bounding boxes are unsuitable. In lane detection, anchors are often preset starting points and lines with different slopes, with the network predicting the relative distance between the lane and the anchor to optimize shape and position [16]–[22]. These innovations improve accuracy and efficiency in complex or occluded scenarios.

Research on downstream tasks in adverse weather conditions [23], such as fog, is limited compared to other detection and segmentation tasks. Traditional solutions often use image enhancement techniques, like dehazing, to improve visual clarity, but this doesn't always lead to better detection results. Some methods combine image enhancement with detection to reduce weather interference [24], while others simulate foggy images to augment datasets. For example, Nie et al. [25] generated foggy images from clear lane images in the CULane dataset, achieving synthetic data augmentation that improved recognition rates from 76.65% to 86.65% under light fog.

Domain adaptation techniques also address the style gap between foggy and clear-weather images [26], [27]. Hnawa et al. [28] proposed a multi-scale domain-adaptive YOLO model, while Li et al. [29] introduced a transfer learning framework

for fog-adaptive object detection using labeled clear-weather and unlabeled foggy images, avoiding the need for annotated foggy datasets.

Traditional dehazing methods suffer from artifacts, whereas deep learning methods using CNNs capture more complex features but require high computational resources and diverse training datasets. However, obtaining real paired images under foggy conditions is challenging, and synthetic images often lead to reduced performance in real-world scenarios.

Lane detection is a critical component of Advanced Driver Assistance Systems (ADAS), supporting key functionalities such as lane departure warnings and autonomous navigation. While existing lane detection algorithms perform well under clear weather conditions with visible lane markings, their performance drops significantly in adverse environments like fog, where reduced visibility and image degradation obscure lane clarity, thus increasing the risk of traffic accidents. Furthermore, the lack of specialized datasets tailored to foggy conditions has limited the development of effective deep learning-based solutions for these challenging scenarios.

To address these limitations, we introduce the FoggyLane dataset, a new benchmark specifically designed for lane detection under foggy conditions. This dataset, comprising 1,423 annotated images across six distinct foggy road scenarios, fills a crucial gap in the current lane detection datasets. In addition, we generate foggy versions of two widely-used lane detection datasets, CULane [8] and Tusimple [30], creating FoggyCULane and FoggyTusimple datasets. These datasets

are essential for training and testing lane detection algorithms in foggy environments.

In response to the unique challenges posed by foggy conditions, we propose a robust real-time lane detection method optimized for such environments. The main contributions of our work are as follows:

- 1) To address the issue of missing global information in foggy images, we design a Global Feature Fusion Module (GFFM) within the backbone network to capture relationships between inputs, improving feature extraction in foggy scenarios.
- 2) To enhance the utilization of structural relationships between lane instances, we introduce a Kernel Feature Fusion Module (KFFM) that learns and predicts the correlations between lane instances, improving lane detection accuracy and robustness.
- 3) To tackle the loss of edge information in foggy images, we incorporate a Low-level Edge Enhancement Module (LEEM) that enhances the model's attention to edge features, improving the accuracy and stability of lane detection.
- 4) To address the lack of open-source foggy lane detection datasets, we construct FoggyLane, a real-world dataset with 1,423 annotated images, and generate FoggyCU-Lane and FoggyTusimple based on existing datasets. Our method achieves state-of-the-art performance with inference speeds of 192.9 FPS on NVIDIA RTX 3090 and 38.4 FPS on NVIDIA Jetson AGX Orin, confirming its real-time capability and practical applicability in real-world settings.

## II. RELATED WORK

In recent years, advances in deep learning have substantially improved lane detection performance. Building on these advances, current approaches for lane detection can be categorized into four main paradigms based on their modeling principles: segmentation-based, anchor-based, curve-based, and row-wise-based methods.

### A. Segmentation-based Lane Detection

Segmentation-based methods mainly utilize semantic segmentation or instance segmentation techniques to distinguish lane lines from other objects or backgrounds in the image, transforming lane detection into a pixel-level classification problem. LaneNet [5] employs a two-branch structure of split branches and embedded branches, the split branches output a binary lane mask to recognize lane lines, and the embedded branches assign a unique embedding to each pixel to realize the distinction of lane lines. SCNN [8] extends the traditional layer-by-layer convolution operation with a slice-by-slice convolution operation, which passes the information horizontally and vertically between the pixels within a layer, thus enhancing the continuity of lane line recognition. RESA [31] introduces a spatial attention module that ensures robust lane prediction by cyclically shifting the feature map horizontally and vertically so that each pixel can acquire global

information. Although these segmentation-based methods possess high accuracy and robustness, the models are bulky and slow to process due to high consumption of computational resources. HW-Transformer [32] presents an innovative lane detection network that utilizes row and column multi-head self-attention to expand the visual range around the lane and enable global information communication through intersecting features, alongside a self-attention knowledge distillation (SAKD) method to enhance performance and semantic feature learning.

### B. Curve-based Lane Detection

Curve-based methods transform the lane detection into a regression task by predicting polynomial coefficients that fit lane lines to polynomial equations. PolyLaneNet [33] introduces an end-to-end convolutional neural architecture that maps from images to polynomials representing each lane marker in the image, as well as domain lane polynomials and confidence scores for each lane. LSTR [34] can also directly output the parameters of the lane shape model, has developed a Transformer-based network that takes into account non-local interactions, enabling it to capture the narrow structure of the lane lines and global context information. DBNet [35] introduces NURBS curves and utilizes their geometric semantic properties to achieve local and global optimization, which improves the robustness of lane line detection and model interpretation. However, polynomial fitting is sensitive to parameter selection, and minor changes in parameters can result in significant variations in fitting results, leading to unstable lane line detection. PGA-Net [36] introduces an end-to-end framework for lane detection, utilizing cubic polynomial functions and a transformer-based DETR model to simultaneously predict lane shape parameters and incorporate global road context, with the addition of Mean Curvature Loss to enhance the accuracy of curve predictions.

### C. Anchor-based Lane Detection

Anchor-based approaches employ predetermined reference lines within the image space to generate lane predictions, subsequently calculating necessary offsets to precisely match these anchors with true lane markings. Line-CNN [37] introduces the anchor mechanism into lane detection for the first time, and innovatively proposes line anchors. LaneATT [17] effectively solves the problem of occlusion and illumination due to the lack of a line anchor, by fusing extracted anchor features with global features generated by attention module. CLRNet [18] employs a coarse-to-fine detection strategy, where lane lines are first approximated using high-level semantic cues before being refined with detailed low-level features. This hierarchical fusion of semantic information significantly improves detection precision. FLAMNet [19] employs an adaptive line anchor strategy, augmented by patch-based feature pooling and decomposed self-attention mechanisms. This design strengthens both local feature extraction and global context modeling, improving performance in handling intricate lane structures. However, due to the multiple curvature and orientation variations of lane lines in the real world, the

performance of the anchor-based methods may be limited in capturing precise paths with complex shapes.

#### D. Row-wise-based Lane Detection

Row-wise methods predict lane positions for each image row. E2E-LMD [38] first proposes the row-wise-based lane detection task and designs an end-to-end architecture that directly outputs the lane marker positions. UFLD [11] utilizes global features to select the lane positions of predefined rows of an image and proposes a structural loss function, so as to ensure the continuity and smoothness of the lanes. Cond-LaneNet [39] utilizes conditional convolution and row-by-row prediction strategies to enhance lane recognition accuracy, and introduces the RIM module to effectively address complex lane layouts. The row-wise-based detection methods improve computational efficiency by focusing only on the row regions in the image, and possesses high detection accuracy while maintaining efficiency.

### III. DATA CONSTRUCTION

Due to the data-driven nature of deep learning models, the quality, size, and diversity of the datasets largely determine the applicability and performance of such models. In the task of lane detection, models trained solely on clear weather data struggle to adapt to low-visibility foggy conditions. Issues such as blurred lane boundaries, faded lane colors, and reduced image quality often arise in fog, making lane detection more challenging. Therefore, training with a foggy weather lane dataset can significantly improve an autonomous driving system's ability to handle such conditions, enhancing both detection accuracy and overall reliability. However, there is currently no publicly available foggy weather lane detection dataset. To address this gap, we have collected and constructed a foggy weather lane detection dataset called FoggyLane. In addition, we generated two supplementary datasets, FoggyCULane and FoggyTusimple, by using fog modeling techniques on existing CULane [8] and Tusimple [30] datasets to test the generalizability of our methods.

#### A. FoggyLane

Existing lane detection algorithms for intelligent connected vehicle ADAS systems perform well under favorable weather conditions, but their performance significantly deteriorates in adverse conditions like fog, which reduces visibility and increases the likelihood of traffic accidents. Current benchmark datasets, including CULane [8], Tusimple [30], and LLAMAS [41], lack foggy weather data. To address this, we developed FoggyLane, a dataset specifically designed for foggy conditions. Data was collected using a monocular forward-facing camera at various times and locations, including Suzhou and Urumqi, China, between October 2023 and January 2024. The dataset includes 1,086 images at various resolutions, which were resized to  $1640 \times 590$  for consistency.

Since foggy conditions are rare, we extended the dataset by incorporating foggy driving scenes from two YouTube videos [42], resulting in an additional 337 images. The final

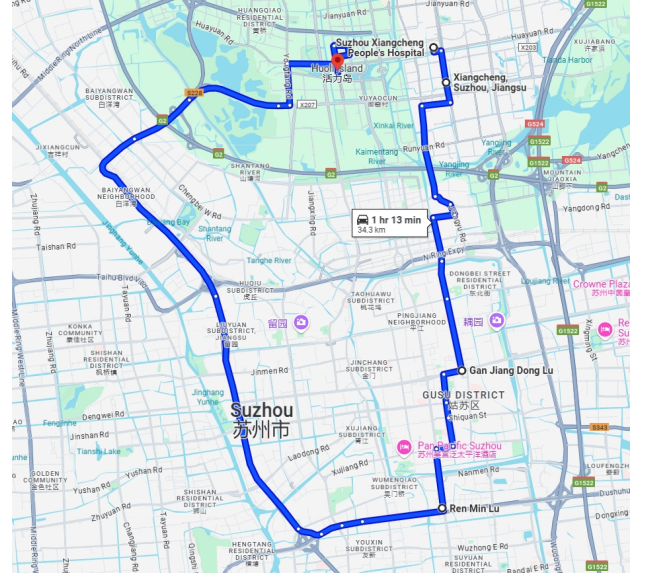


Fig. 2. The route for dataset acquisition in Suzhou on the morning of October 26, 2023. [40]

FoggyLane dataset contains 1,423 images, covering six road scenes: Normal, Arrow, Crowd, Curve, Night, and Crossroad. We split the dataset into training and testing sets at a 2:1 ratio, ensuring balanced distribution across scene types.

Comparing FoggyLane with existing datasets, such as Caltech-Lanes [43] and Tusimple [30], which focus on single traffic scenarios, and LLAMAS [41], which uses high-precision map annotations, we found that these datasets do not cover foggy weather scenarios. While ApolloScape [44] and BDD100k [45] include multiple traffic scenarios, they lack instance-level annotations. Similarly, although CULane [8] and CurveLanes [46] cover a wide range of traffic scenes, they do not include foggy conditions. Models trained on datasets limited to clear weather struggle in fog, where lane boundaries are blurred and image quality reduced. To address this gap, FoggyLane provides a comprehensive solution for foggy weather lane detection with instance-level annotations, available in both Tusimple [30] and CULane [8] formats for broader accessibility.

Our dataset has two key advantages:

- 1) **Pioneering foggy lane detection dataset:** FoggyLane is a dataset specifically designed to address foggy weather scenarios. It covers a range of challenging conditions, including foggy congested roads, foggy curves, and foggy night roads. This dataset is crucial for testing the robustness of ADAS under adverse conditions.
- 2) **Strict annotation standards:** The dataset follows strict annotation guidelines, including marking the center of lanes, connecting lane markings at intersections, and prioritizing solid lines over grid lines, etc. [47]. These rigorous annotations can significantly improve the accuracy and consistency of lane detection in foggy weather, thus enhancing the stability and safety of autonomous driving systems and providing a solid data foundation for the reliable deployment of autonomous technology.



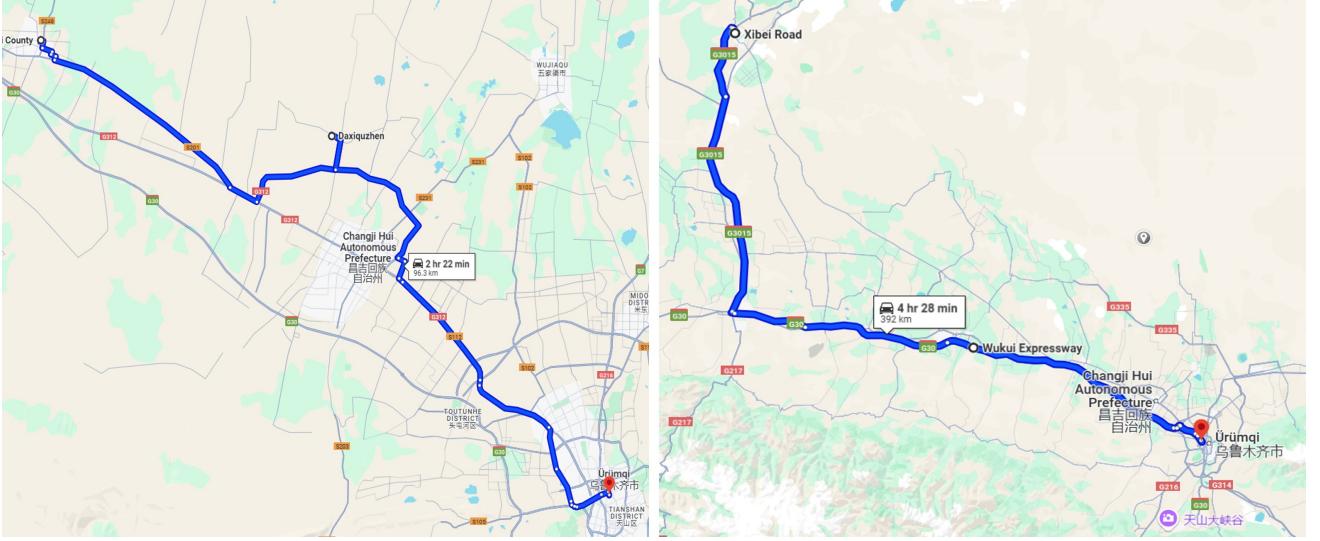


Fig. 3. The routes for dataset acquisition in Urumqi, Xinjiang Autonomous Region: the left illustrates the morning of December 9, 2023, while the right depicts the evening of January 2, 2024. [40]

TABLE I  
COMPARISON BETWEEN OUR DATASET AND EXISTING LANE DETECTION DATASETS

Dataset	Frames	Multi-traffic scenarios	Instance-level annotation	Number of foggy datasets	Resolution
Caltech-Lanes [43]	1.2k	✗	✓	None	640 x 480
Tusimple [30]	6.4k	✗	✓	None	1280 x 720
LLAMAS [41]	100k	✓	✓	None	1276 x 717
Appolloscape [44]	110k	✓	✗	None	3384 x 2710
BDD100k [45]	100k	✓	✗	None	1280 x 720
CULane [8]	133k	✓	✓	None	1640 x 590
CurveLanes [46]	150k	✓	✓	None	1280 x 720
FoggyLane (ours)	1.5k	✓	✓	1.5k	1640 x 590

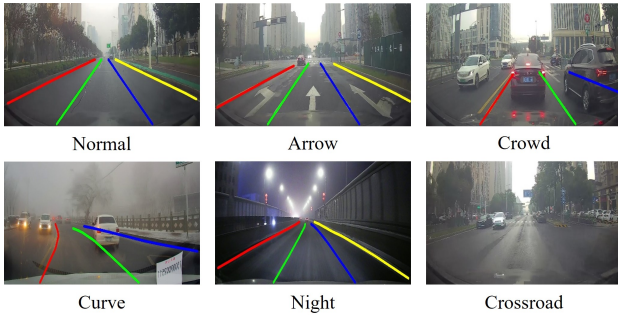


Fig. 4. The different road types of FoggyLane images examples.

### B. FoggyCULane and FoggyTusimple

Currently, numerous datasets are available for lane detection. Among them, we select two widely adopted and representative benchmarks: CULane [8] and TuSimple [30]. The CULane dataset [8] is a large-scale and challenging benchmark that covers diverse scenarios including highways, urban streets, and rural areas in Beijing. In contrast, the TuSimple dataset [30] primarily comprises daytime driving videos collected on American highways, featuring a variety of lighting conditions

and complex traffic situations. Based on these datasets, we generate synthetic foggy versions, named FoggyCULane and FoggyTuSimple, to facilitate evaluation under adverse weather conditions.

The method for generating foggy images is inspired by the model [25], and the specific generation method is provided in the Supplementary Material for Review. As shown in Figure 5, it demonstrates the generation case of FoggyCULane.

## IV. METHODS

### A. Overall structure

To address the challenge of lane detection in foggy conditions, where visibility is significantly reduced, we propose a fog-enhanced lane detection network inspired by row-wise methods. As illustrated in the Fig. 6, the network comprises three main components: a backbone network, a neck network, and a detection head. To mitigate the loss of global information in foggy images, we introduce a global feature fusion module within the backbone network. In the neck network, we utilize HRNetV2 [48] to further integrate multi-scale features from different stages of the backbone, enabling the aggregation of information across various scales and resolutions.

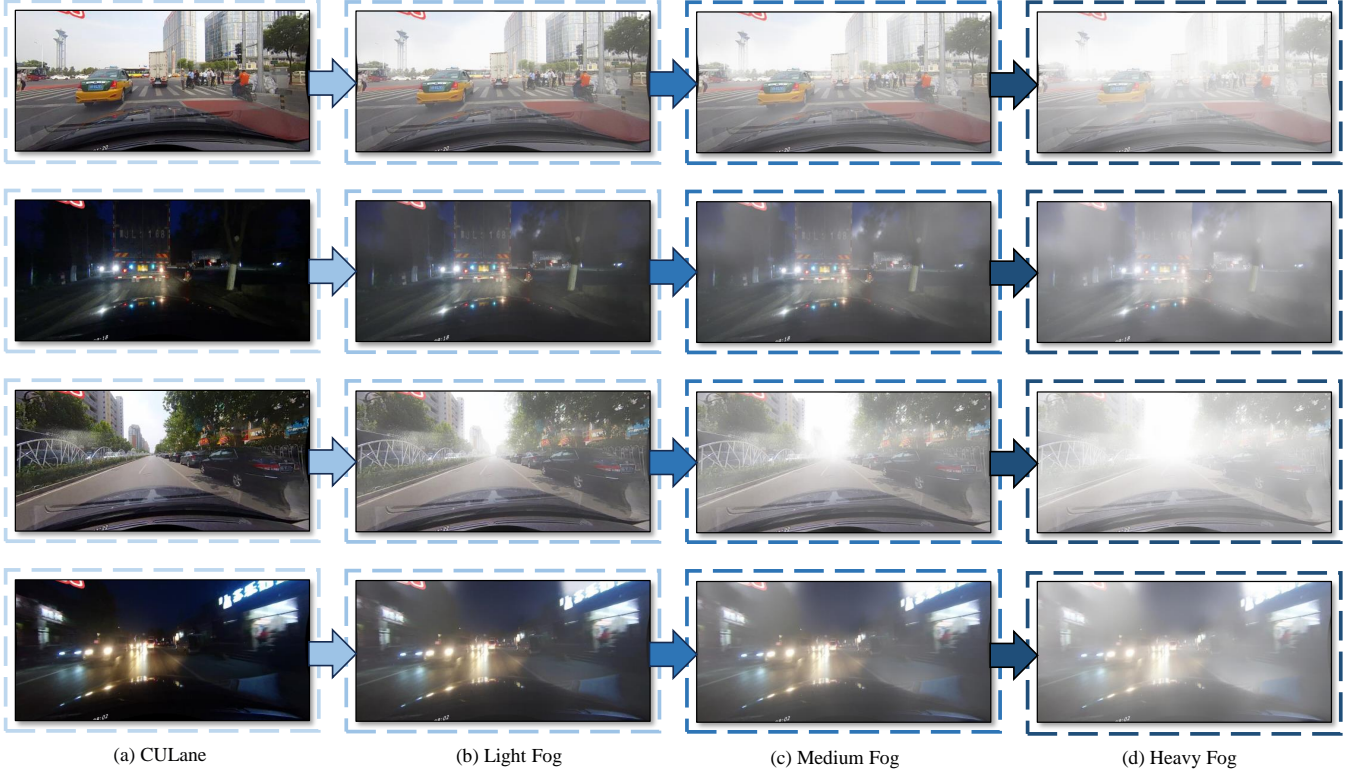


Fig. 5. The FoggyCULane dataset examples.

For the detection head, we employ the concept of dynamic convolution, incorporating both lane instance detection and lane mask segmentation. During instance detection, the network identifies lane instances within the image and predicts a set of dynamic convolution kernel parameters for each lane. These parameters are subsequently applied to the lane mask segmentation head to filter the instance-specific segmentation map for each lane. This approach eliminates the need for complex post-processing steps, enhancing detection speed.

Moreover, to fully exploit the structural relationships between lane lines, we designed a kernel feature fusion module, which allows the network to automatically learn the correlations between predicted lane instances. This contributes to more accurate lane identification and localization. Additionally, to compensate for the loss of edge information in foggy images, we incorporated a low-level edge enhancement module, further improving the network’s ability to detect lane boundaries with precision.

### B. Global Feature Fusion Module

In recent years, Transformer models have achieved significant success in natural language processing, leading researchers to explore their applications in computer vision. With self-attention mechanisms, Transformer models can capture dependencies between different regions and pixels within an image, thus facilitating a better understanding of global image information. As a result, Transformer models have demonstrated outstanding modeling capabilities and performance improvements in various traffic vision tasks [49]–[51]. However,

applying Transformers to the visual domain still faces some challenges. Firstly, traditional Transformer architectures lack the hierarchical structure and down-sampling operations found in CNN models, making them less adaptable to changes in resolution and receptive field, which may hinder handling of complex visual entities. Additionally, calculating global attention at high resolutions can be computationally intensive.

To address these issues, researchers have proposed several enhanced architectures, such as hierarchical Transformers [52]–[54]. Among them, the Swin Transformer [52] combines CNN-inspired concepts, integrating local perception with global attention in a hierarchical Transformer framework. As the Swin Transformer has shown strong performance in classification, detection, and segmentation tasks, balancing computational efficiency with accuracy, we chose the Swin Transformer as our backbone network. However, since the Swin Transformer’s window attention mechanism primarily focuses on local features, its hierarchical structure may still lack sufficient global context for foggy scene understanding. Therefore, as illustrated in the Fig. 7, we designed a Global Feature Fusion Module (GFFM) to enhance the network’s global information integration. Specifically, we replaced the window attention mechanism in the final stage with a standard multi-head attention mechanism to capture global correlations across all inputs. At this stage, image resolution has been sufficiently reduced, making the computational cost of global attention manageable.

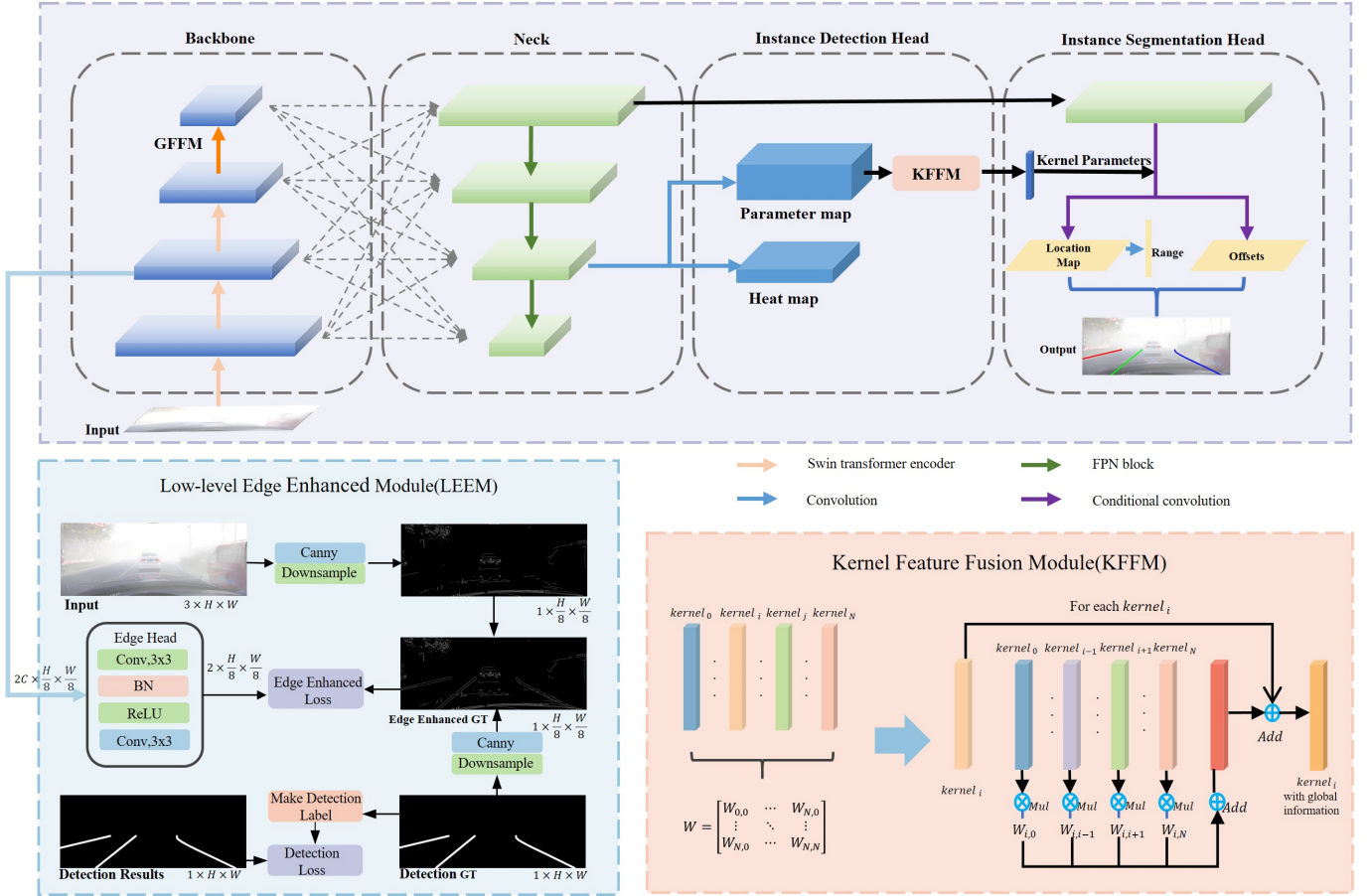


Fig. 6. Overview of the proposed network.

### C. Kernel Feature Fusion Module

Dynamic convolution adjusts convolutional kernel parameters based on input data, enhancing network flexibility and generalization compared to traditional convolution. CondInst [55] is an instance segmentation framework using dynamic convolution to generate kernel parameters for each instance, reducing network load and improving efficiency. Similarly, CondLane [39] applies dynamic convolution for lane instance segmentation, achieving strong performance.

Building on this, our lane detection head also uses dynamic convolution, consisting of lane instance detection and mask segmentation. Unlike traditional methods, we generate dynamic convolution kernels using the lane's starting position features rather than center features, which are more suitable for the elongated nature of lanes. We design an instance detection head with two branches: one predicts lane starting points and generates a heatmap, and the other generates dynamic convolution kernels for lane segmentation.

However, existing methods don't fully utilize the structural relationships between lane instances. To address this, we introduce a Kernel Feature Fusion Module (KFFM) that enables the network to learn and predict relationships between lane instances, enhancing detection performance. KFFM is shown in the bottom right of Fig. 6.

### D. Low-level Edge Enhanced Module

Images in foggy conditions differ from those captured under good lighting primarily due to their blurriness and low contrast. This effect renders the edges of objects and details within the scene indistinct and hard to detect, impacting the algorithm's ability to understand and recognize the scene accurately. Edge information, beyond simply marking object boundaries, also implicitly contains structural and spatial information about objects, forming a critical foundation for tasks such as object detection, segmentation, and tracking. Using the Canny edge detection algorithm with identical threshold settings, we processed both foggy and normal images, as shown in the Fig. 8. It is evident that fog significantly degrades edge information, particularly affecting lane line edges, which become nearly indiscernible. Given that lane detection relies heavily on edge information—lane positioning is typically determined by the boundary between lane edges and the road background—both global scene information and detailed edge information are essential for accurate lane detection. To address the challenges of lane detection in foggy conditions, we apply global feature fusion within both the backbone network and detection head to enhance high-dimensional global features. Additionally, we use multi-scale fusion to aggregate detail features from low-resolution feature maps. However, this approach alone does not fully compensate for the loss of edge detail inherent in foggy images. Therefore, we introduce a



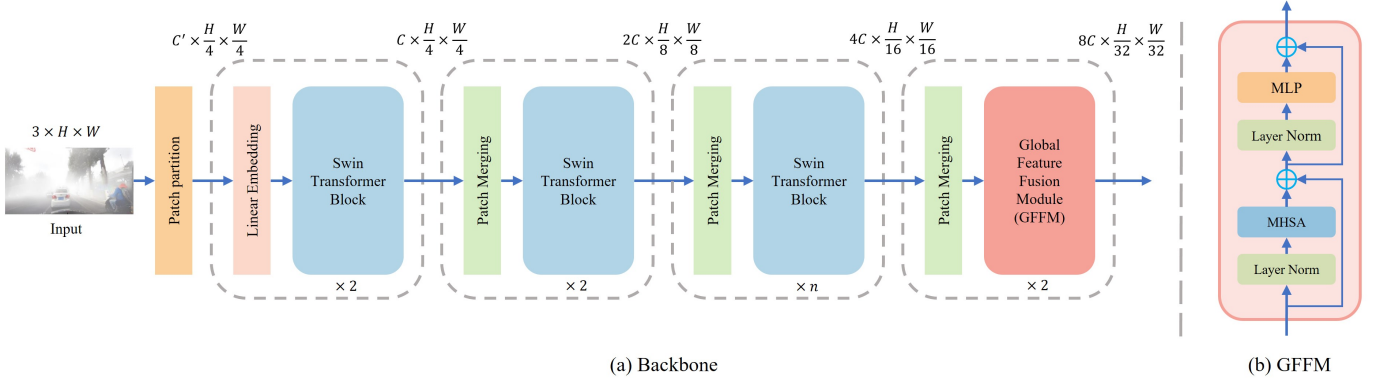


Fig. 7. Backbone Network with Global Feature Fusion. The Swin Transformer’s window attention mechanism mainly focuses on local features. Although its layered structure increases the receptive field, it may still fall short in understanding foggy scenes. To address this, we designed a Global Feature Fusion Module (GFFM), replacing the final stage’s window attention with standard multi-head attention to capture global relationships.



Fig. 8. Comparison of edge information between foggy and normal scenarios.

Low-level Edge Enhanced Module (LEEM) into the network to boost the network’s focus on edge information, thereby improving both the accuracy and stability of lane detection.

Specifically, we add an auxiliary path in the network to learn the edge features of the input image. First, we apply the Canny

operator to the input image for edge detection, supplemented by lane line labels to reconstruct any missing lane edges, generating the training labels for the edge enhancement module. To avoid interfering with high-level semantic extraction and subsequent detection segmentation, while strengthening the low-level network’s learning of edge textures and other low-dimensional features, we introduce a branch at the second stage of the backbone network. This branch sequentially applies a  $3 \times 3$  and a  $1 \times 1$  convolution. We then compute the cross-entropy loss between the branch output and the edge labels. The detailed structure is illustrated in the bottom-left of the Fig. 6. Notably, this auxiliary enhancement path is only active during training, thus not increasing computation or processing time during deployment.

TABLE II  
COMPARISON WITH ADVANCED LANE DETECTION ON FOGGYLANE DATASET.

Method	Venue	Backbone	F1@50	F1@65	F1@75	F1@85	mF1	Gflops(G)	FPS
SCNN [8]	AAAI 2018	VGG16	84.01	62.08	56.34	12.76	41.78	328.4	18.7
UFLD [11]	ECCV 2020	ResNet18	81.76	56.54	32.32	6.50	38.24	8.4	327.3
UFLD [11]	ECCV 2020	ResNet34	82.75	61.25	34.44	7.89	40.23	16.9	176.9
LaneATT [17]	CVPR 2020	ResNet18	81.98	59.61	34.78	7.69	40.06	9.3	247.7
LaneATT [17]	CVPR 2020	ResNet34	84.32	63.08	38.91	10.76	42.63	18.0	167.1
LaneATT [17]	CVPR 2020	ResNet122	86.25	72.42	51.50	17.26	48.95	70.5	28.6
LSTR [34]	WACV 2021	ResNet34	83.79	68.23	58.29	25.32	48.91	-	124.4
RESA [31]	AAAI 2021	ResNet34	85.19	65.89	61.89	14.57	48.75	41.0	76.7
RESA [31]	AAAI 2021	ResNet50	86.24	69.22	65.27	16.55	52.34	43.0	53.0
CondLane [39]	ICCV 2021	ResNet18	90.38	75.08	47.50	47.50	10.96	10.2	194.7
CondLane [39]	ICCV 2021	ResNet34	90.58	78.45	56.48	15.59	52.25	19.6	136.5
CondLane [39]	ICCV 2021	ResNet101	91.54	82.09	65.30	30.68	57.76	44.8	60.2
CLRNet [18]	CVPR 2022	ResNet18	90.96	83.23	68.53	34.78	59.81	11.9	105.0
CLRNet [18]	CVPR 2022	ResNet34	91.56	82.43	65.61	30.20	58.14	21.5	90.0
CLRNet [18]	CVPR 2022	ResNet101	91.58	85.19	73.38	41.02	64.47	42.9	47.7
CLRNet [18]	CVPR 2022	DLA34	92.09	83.98	72.15	41.61	62.28	18.5	81.3
FLAMNet [19]	IEEE TITS 2023	ResNet34	89.94	78.90	55.32	12.96	50.99	30.1	32.0
FLAMNet [19]	IEEE TITS 2023	DLA34	91.16	82.77	64.95	24.22	56.70	21.7	31.7
DBNet [35]	IEEE TIV 2024	ResNet18	89.61	81.27	65.27	26.15	56.52	22.64	147.6
DBNet [35]	IEEE TIV 2024	ResNet34	90.02	83.44	71.66	40.51	60.94	32.1	129.0
HWLane [32]	IEEE TITS 2024	Res34	91.99	84.23	68.08	35.27	34.38	18.60	70.0
PolarRCNN [21]	IEEE TITS 2025	ResNet34	91.07	79.38	57.44	14.74	52.42	19.04	171.6
PolarRCNN [21]	IEEE TITS 2025	DLA34	90.02	83.44	71.66	40.51	51.97	16.05	150.4
Ours	-	SwinGFFM-t	92.34	84.65	70.99	35.77	60.82	12.0	70.4 / 304.7*
Ours	-	SwinGFFM-s	<b>95.04(2.95↑)</b>	<b>88.61(3.42↑)</b>	<b>77.32(3.94↑)</b>	<b>45.02(3.41↑)</b>	<b>65.60(3.13↑)</b>	20.3	38.2 / 192.9*

Note: For a fairer comparison, we re-evaluated the FPS of the source code available detectors using one NVIDIA GeForce RTX 3090 GPU on the same machine. \* indicates the FPS after acceleration with TensorRT.





Fig. 9. Visualization results of CLNet [18], FLAMNet [19], PolarRCNN [21] and our method on FoggyLane testing set. The arrows indicate instances of lane lines that were not correctly detected by the corresponding method.

### E. Loss functions

Based on the above, our method involves a total of five prediction tasks: lane start point prediction, row-based segmentation prediction, vertical range prediction, offset prediction, and edge prediction. The loss functions for each task are detailed below.

1) *Lane start point prediction*: In feature maps with a large receptive field and low resolution, the lane line start point is difficult to be accurately represented by a single pixel location. Moreover, in such large receptive field feature maps, pixels near the target point exhibit similar features. If these pixels are directly labeled as negative samples, it will interfere with the network training and make it difficult for the network to

learn and optimize. Therefore, this method uses a Gaussian kernel function to generate a heatmap label for the lane line start point. Each element in the heatmap label represents the confidence that the position corresponds to the target point; the closer to the target point, the higher the confidence, and the farther away, the lower the confidence. In other words, the ground truth is softly labeled with a Gaussian function, making it easier for the network to converge. Suppose  $(x, y)$  denotes a position on the low-resolution feature map, and  $(p_x, p_y)$  represents the coordinate of the target point on the low-resolution feature map. Then, the ground truth heatmap

TABLE III  
COMPARISON WITH ADVANCED LANE DETECTION ON FOGGYCULANE DATASET

Method	Venue	Backbone	Normal	Crowded	Dazzle light	Shadow	No line	Arrow	Curve	Cross	Night	Total
SCNN [8]	AAAI 2018	VGG16	91.07	71.32	67.23	65.23	49.14	88.06	67.07	1344	70.78	72.94
UFLD [11]	ECCV 2020	ResNet18	87.57	65.47	55.21	60.38	38.66	82.26	57.29	1849	60.61	67.69
UFLD [11]	ECCV 2020	ResNet34	89.10	68.29	60.91	62.03	41.98	85.17	63.88	2371	70.13	70.13
LaneATT [17]	CVPR 2020	ResNet18	90.52	71.52	65.70	68.92	47.31	86.32	62.34	870	67.64	74.30
LaneATT [17]	CVPR 2020	ResNet34	91.68	72.93	67.23	65.23	49.14	88.06	67.07	1344	70.78	75.53
LaneATT [17]	CVPR 2020	ResNet122	91.12	74.68	68.87	78.61	47.33	85.76	63.88	1008	69.72	76.16
LSTR [34]	WACV 2021	ResNet34	85.79	63.45	56.73	58.72	38.20	79.31	55.34	1068	57.62	65.64
RESA [31]	AAAI 2021	ResNet34	90.97	72.32	67.31	74.01	46.52	86.32	65.26	1536	73.62	74.97
RESA [31]	AAAI 2021	ResNet50	92.09	73.49	67.40	73.87	47.92	87.48	69.28	1722	69.85	75.19
CondLane [39]	ICCV 2021	ResNet18	91.56	74.41	71.12	77.89	48.59	86.73	71.34	1262	71.00	76.46
CondLane [39]	ICCV 2021	ResNet34	91.76	75.55	69.62	74.62	50.01	87.40	71.29	1427	72.11	77.06
CondLane [39]	ICCV 2021	ResNet101	92.47	76.26	70.91	78.50	51.84	88.93	72.51	1597	72.75	77.90
CLNet [18]	CVPR 2022	ResNet18	92.55	76.47	71.89	74.45	50.82	88.94	65.93	1122	72.86	78.04
CLNet [18]	CVPR 2022	ResNet34	92.96	76.32	73.40	79.06	51.46	89.39	71.83	1301	73.64	78.36
CLNet [18]	CVPR 2022	ResNet101	92.95	76.67	71.49	79.89	52.47	89.29	68.72	1101	74.03	78.72
CLNet [18]	CVPR 2022	DLA34	93.23	77.64	73.90	79.23	52.11	89.45	72.48	1109	73.63	79.04
FLAMNet [19]	IEEE TITS 2023	ResNet34	92.60	76.61	71.42	79.81	50.89	89.04	71.47	1073	74.17	78.45
FLAMNet [19]	IEEE TITS 2023	DLA34	92.98	77.26	71.84	79.76	51.29	89.34	71.38	1143	73.93	78.77
DBNet [35]	IEEE TIV 2024	ResNet18	84.91	69.27	60.86	67.94	45.69	79.04	67.50	1045	68.57	71.33
DBNet [35]	IEEE TIV 2024	ResNet34	85.61	69.35	61.22	66.50	45.73	79.19	66.51	<b>837</b>	69.93	71.87
HWLane [32]	IEEE TITS 2024	Res34	90.85	73.32	67.18	75.32	47.18	87.14	63.38	1456	69.20	74.61
PolarRCNN [21]	IEEE TITS 2025	ResNet34	93.34	77.76	<b>75.26</b>	79.76	53.25	89.62	75.94	1289	74.54	78.68
PolarRCNN [21]	IEEE TITS 2025	DLA34	92.90	77.50	74.03	80.89	51.71	89.76	73.02	1226	74.21	79.13
Ours	-	SwinGFFM-t	92.68	77.50	71.52	80.42	50.95	88.92	72.08	950	73.11	78.66
Ours	-	SwinGFFM-s	<b>93.40(0.17↑)</b>	<b>78.63(1.99↑)</b>	73.89	<b>82.74(2.85↑)</b>	<b>53.75(1.28↑)</b>	<b>89.82(0.37↑)</b>	<b>74.09(1.58↑)</b>	1146	<b>74.97(0.80↑)</b>	<b>79.85(0.72↑)</b>

Note: Our method attains state-of-the-art (SOTA) results in multiple scenarios including Normal, Crowded, Shadow, No-line, Arrow, Curve and Night conditions, as well as in the overall (Total) performance.

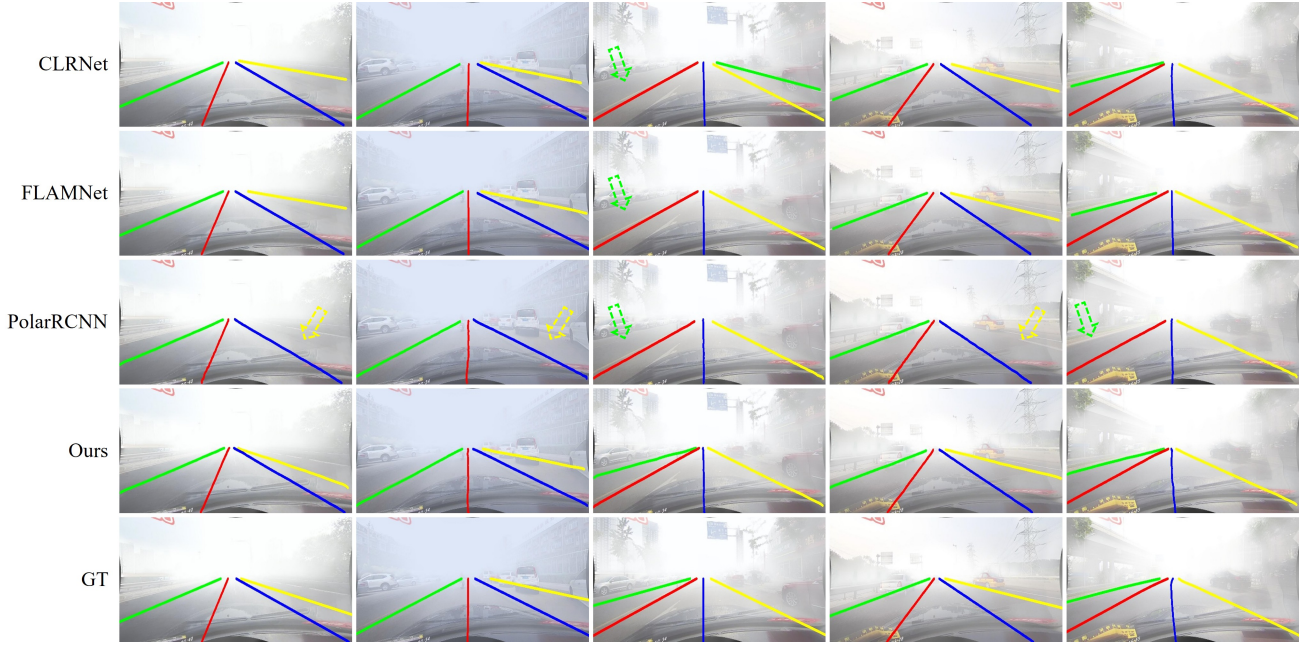


Fig. 10. Visualization results of CLRNet [18], FLAMNet [19], PolarRCNN [21] and our method on FoggyCULane testing set. The arrows indicate instances of lane lines that were not correctly detected by the corresponding method.

$GT$  value at position  $(x, y)$  is defined as:

$$GT(x, y) = \exp\left(-\frac{(x - p_x)^2 + (y - p_y)^2}{2\sigma^2}\right) \quad (1)$$

where  $\sigma$  controls the decay rate of the Gaussian kernel. A larger  $\sigma$  results in slower confidence decay and thus a larger heatmap area.

This method combines the Gaussian heatmaps of all lane line start points within the image into a single heatmap. When multiple heatmaps respond at the same location, the maximum value is retained to form the final ground truth heatmap. Then, the Focal Loss is used to calculate the loss between the predicted heatmap and the ground truth heatmap. Let the predicted heatmap value at position  $(x, y)$  be  $P_{xy}$ , and let  $N$  be the total number of pixels in the heatmap. The Focal Loss between the predicted heatmap and the ground truth heatmap is defined as:

$$\mathcal{L}_{hm} = -\frac{1}{N} \sum_{x,y} \begin{cases} (1 - P_{xy})^\alpha \log(P_{xy}), & \text{if } GT(x, y) = 1 \\ (1 - GT(x, y))^\beta (P_{xy})^\alpha \log(1 - P_{xy}), & \text{otherwise} \end{cases} \quad (2)$$

2) *Row-based segmentation prediction:* Row-based segmentation predicts a horizontal coordinate  $E(\hat{x}_i)$  for each row. For this task, our method uses the L1 loss function to optimize the predicted coordinates. Suppose  $V$  denotes the effective vertical range of the lane line,  $N_v$  is the number of effective rows, and  $x_i$  is the ground truth horizontal coordinate. The loss function is defined as:

$$L_{row} = \frac{1}{N_v} \sum_{i \in V} |E(\hat{x}_i) - x_i| \quad (3)$$

3) *Vertical range prediction:* For the label of the lane line vertical range vector prediction, our method uses a  $1 \times Y$  vector representation. If the lane line passes through the  $Y_i$

row, its value is 1; otherwise, it is 0. Thus, this can be regarded as a segmentation task. Our method optimizes it using the cross-entropy loss function. Suppose  $v_i$  denotes the predicted probability that the  $i$ -th row is positive, then the loss function is defined as:

$$L_{range} = \sum (-y_{gt}^i \log(v_i) - (1 - y_{gt}^i) \log(1 - v_i)) \quad (4)$$

4) *Offset prediction:* Firstly, the generation of ground truth labels for offset prediction is required. For each lane line, the proposed method constructs the ground truth offset as the horizontal displacement relative to the lane centerline for each grid cell within a specified width. The predicted offsets are optimized using an L1 loss function. Let  $\delta_{xy}$  denote the ground truth offset at coordinate  $(x, y)$ ,  $\hat{\delta}_{xy}$  the predicted offset, and  $\Omega$  the region surrounding the lane line. The loss function is then formulated as follows:

$$L_{offset} = \frac{1}{N_\Omega} \sum_{(x,y) \in \Omega} |\hat{\delta}_{xy} - \delta_{xy}| \quad (5)$$

5) *Edge prediction:* For the task of edge enhancement, the method treats it as an edge segmentation problem, which is essentially a binary classification task. The labels at edge locations are assigned a value of 1, while non-edge locations are assigned 0. Accordingly, the cross-entropy loss function is employed for optimization. Let  $e_{gt}^i$  denote the label of pixel  $i$ , and  $p_i$  represent the predicted probability of the pixel being positive. The loss function is defined as:

$$L_{edge} = \sum_i (-e_{gt}^i \log(p_i) - (1 - e_{gt}^i) \log(1 - p_i)) \quad (6)$$

6) *Total loss:* To balance the influence of different tasks on the overall training of the network, a weighted fusion of the loss functions for each sub-task is employed. The total loss function is formulated as follows:

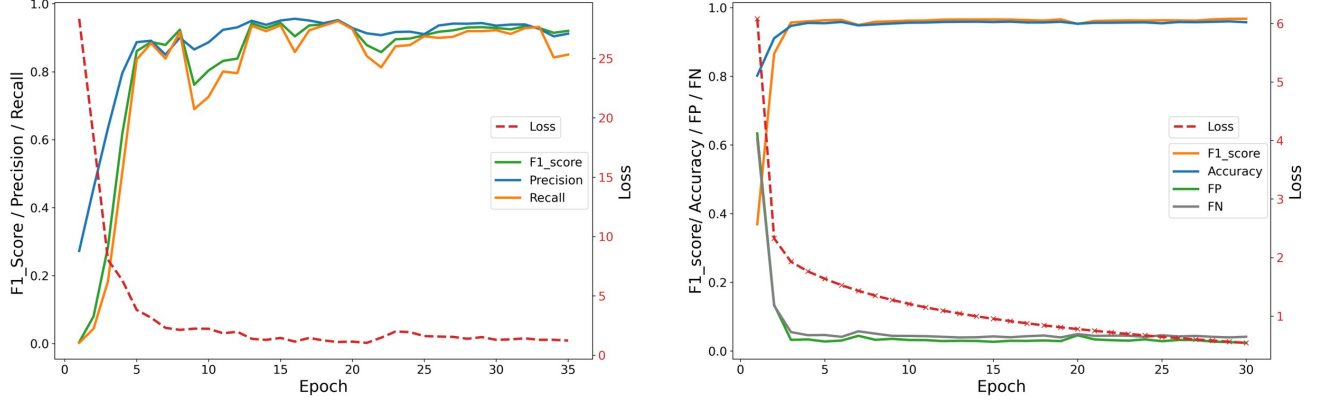


Fig. 11. Several metrics of our model’s performance during the training process on the FoggyLane and FoggyTusimple datasets, with results on FoggyLane on the left and FoggyTusimple on the right.

$$L_{\text{total}} = \alpha L_{hm} + \beta L_{\text{row}} + \gamma L_{\text{range}} + \delta L_{\text{offset}} + \varepsilon L_{\text{edge}} \quad (7)$$

where the network achieves optimal performance when the weights are set as  $\alpha = 1$ ,  $\beta = 1$ ,  $\gamma = 1$ ,  $\delta = 0.4$ , and  $\varepsilon = 0.1$ .

## V. EXPERIMENTS

### A. Datasets

In the Data Construction chapter, we introduce the FoggyLane dataset, which was constructed from real-world collections for foggy lane detection, along with the FoggyCULane and FoggyTusimple datasets that were synthesized through modeling foggy images. Our method is evaluated on these three datasets.

FoggyLane is a lane detection dataset specifically designed for foggy scenarios, containing 1,423 frames of foggy lane images for training and testing. All images are of resolution 1640x590 pixels.

FoggyCULane is synthesized from the large-scale challenging lane detection dataset CULane using a foggy image modeling approach. It maintains the same number of images as CULane, which includes 88,880 images for training and 34,680 images for testing. The resolution of all images is also 1640x590 pixels.

FoggyTusimple is synthesized from one of the most widely used benchmark datasets for lane detection, Tusimple, through the foggy image modeling method. At the same time, the dataset follows the same structure as Tusimple, comprising 3,268 training images, 358 validation samples, and 2,782 test cases. All visual data maintains a consistent resolution of 1280x720 pixels.

### B. Evaluation Metric

Lane detection is commonly treated as a semantic segmentation task, evaluated using standard metrics such as True Positive (TP), False Positive (FP), False Negative (FN), and True Negative (TN). However, due to its unique structure, lane detection also adopts specialized metrics. Following SCNN’s

[8] protocol, we connect labeled or predicted lane points into line segments and expand them into 30-pixel-wide areas. A prediction is considered correct if the Intersection over Union (IoU) with the ground truth exceeds 0.5. Based on this, we compute Precision, Recall, and F1-score, with the following formulas:

$$F1 = \frac{2 \times \text{Precision} \times \text{Recall}}{\text{Precision} + \text{Recall}} \quad (8)$$

$$\text{Precision} = \frac{TP}{TP + FP} \quad (9)$$

$$\text{Recall} = \frac{TP}{TP + FN} \quad (10)$$

For the FoggyTusimple dataset, we adopt the evaluation metrics of the Tusimple dataset. The official Tusimple dataset provides three standard evaluation metrics: false positive rate (FPR), false negative rate (FNR), and accuracy. The formula for calculating Accuracy is as follows:

$$\text{Accuracy} = \frac{\sum_{clip} C_{clip}}{\sum_{clip} S_{clip}} \quad (11)$$

where  $C_{clip}$  represents the number of correctly predicted lane points in the image, while  $S_{clip}$  denotes the total number of ground truth lane points. For the pixels in the image, a predicted lane point is considered correct if it falls within 20 pixels to the left or right of the ground truth. Furthermore, if more than 85% of the predicted lane points on a single lane line correspond to the ground truth lane points, the predicted lane is regarded as a true positive.

### C. Implementation Details

We conducted experiments on the NVIDIA GeForce RTX 3090 platform. The SwinGFFM backbone network was pre-trained on the COCO dataset for 500 epochs. During lane detection training, we loaded the pre-trained weights and resized input images to  $800 \times 320$ . Various data augmentation



techniques, including rotation, flipping, brightness adjustment, and random scaling, were applied. The batch size was set to 16, with an initial learning rate of  $3 \times 10^{-4}$ , using the Adam optimizer and a Step learning rate decay. For full network parameters and training details, please refer to our open-source code.

To benchmark against existing methods [8], [11], [17]–[19], [21], [31], [32], [34], [35], [35], [39], we followed the training settings provided in the respective papers. For FoggyCULane and FoggyTusimple, we adopted the training parameters from the original CULane and Tusimple datasets, while for FoggyLane, we extended the training epochs to ensure reliable results.

#### D. Quantitative Results

1) *Results on FoggyLane*: We evaluated our proposed method on the FoggyLane dataset and compared it with other leading lane detection methods. As shown in the Tabel II, we mainly compared the methods in terms of F1 scores, computational complexity (GFlops), processing speed (FPS).

From the Table II, it is evident that our method achieves state-of-the-art performance on the foggy lane detection dataset FoggyLane, with F1@50, F1@65, F1@75, and F1@85 scores of 95.04, 88.61, 77.32, and 45.02, respectively. These results surpass the best-performing alternative methods by margins of 2.95%, 3.42%, 3.94%, and 3.41%. The mean F1 (mF1) score demonstrates a 3.13% improvement over the strongest competing approach. Notably, the SwinGFFM-t variant achieves an F1@50 score of 92.34, which even exceeds the performance of DLA34-based CLRNNet, previously the top-performing method among comparative approaches.

2) *Results on FoggyCULane*: We compared our method with other advanced lane detection methods on the FoggyCULane dataset. As shown in the Table III, our method consistently achieved the best performance across various scenarios, including Normal, Crowded, shadow, No line, Arrow, Night and Curve. Additionally, our model achieved the highest overall F1 score of 79.85, which achieves a 0.72% improvement over the best alternative method.

3) *Results on FoggyTusimple*: As shown in the Table IV, the traffic scenes in the FoggyTusimple dataset are relatively simple, resulting in smaller performance differences between methods. Nonetheless, our method achieved an F1 score of 96.95, outperforming the best existing method by 0.43%. This further demonstrates the effectiveness of our method in foggy conditions.

#### E. Ablation Study

We conducted ablation studies on the FoggyLane and FoggyCULane datasets to evaluate the effectiveness of the GFFM, KFFM, and LEEM modules, using Swin-t as the backbone. As shown in Tables V and VI, each module improves the model's performance. The GFFM module contributes the most, increasing the F1-score by 1.07 on FoggyLane and 0.41 on FoggyCULane, highlighting its ability to capture both local and global information. Adding the KFFM module further boosts the F1-score by 0.63 on FoggyLane and 0.26 on

TABLE IV  
COMPARISON WITH ADVANCED LANE DETECTION ON FOGGYTUSIMPLE DATASET.

Method	Venue	Backbone	F1(%)	ACC(%)	FP(%)	FN(%)
SCNN [8]	AAAI 2018	VGG16	94.64	95.89	5.87	4.78
UFLD [11]	ECCV 2020	ResNet18	94.57	93.60	3.49	7.59
UFLD [11]	ECCV 2020	ResNet34	95.05	95.10	4.84	5.08
LaneATT [17]	CVPR 2020	ResNet18	95.77	95.78	3.83	3.53
LaneATT [17]	CVPR 2020	ResNet34	96.15	95.50	4.59	3.06
LaneATT [17]	CVPR 2020	ResNet122	93.24	95.43	9.61	3.50
LSTR [34]	WACV 2021	ResNet34	94.70	95.58	5.74	4.81
RESA [31]	AAAI 2021	ResNet34	95.22	95.60	4.63	4.95
RESA [31]	AAAI 2021	ResNet50	95.51	95.83	4.53	4.43
CondLane [39]	ICCV 2021	ResNet18	95.41	94.81	3.80	5.46
CondLane [39]	ICCV 2021	ResNet34	95.65	94.69	3.63	5.13
CondLane [39]	ICCV 2021	ResNet101	96.03	95.14	2.94	5.09
CLRNet [18]	CVPR 2022	ResNet18	96.48	95.64	3.89	3.11
CLRNet [18]	CVPR 2022	ResNet34	96.23	95.94	4.34	3.17
CLRNet [18]	CVPR 2022	ResNet101	96.13	95.64	4.15	3.58
FLAMNet [19]	IEEE TITS 2023	ResNet18	96.52	95.65	3.84	3.09
FLAMNet [19]	IEEE TITS 2023	ResNet101	96.34	95.98	4.45	<b>2.82</b>
DBNet [35]	IEEE TIV 2024	ResNet18	95.71	93.89	3.53	5.12
DBNet [35]	IEEE TIV 2024	ResNet34	95.61	93.72	3.48	5.38
HWLANet [32]	IEEE TITS 2024	Res34	95.54	95.91	4.32	4.60
PolarRCNN [21]	IEEE TITS 2025	ResNet34	96.33	95.91	4.50	2.77
PolarRCNN [21]	IEEE TITS 2025	DLA34	96.37	94.99	3.21	4.09
Ours	-	SwinGFFM-t	96.63	95.86	2.77	4.04
Ours	-	SwinGFFM-s	<b>96.95(0.43↑)</b>	<b>96.10(0.12↑)</b>	<b>2.32(0.62↓)</b>	3.83

TABLE V  
ABLATION EXPERIMENTS OF DIFFERENT COMPONENTS ON THE FOGGYLANE DATASET.

Model	GFFM	KFFM	LEEM	F1-score	Gflops(G)
Baseline				90.36	13.77
	✓			91.43	11.94
	✓	✓		92.06	11.97
<b>Ours</b>	✓	✓	✓	<b>92.34↑</b>	12.01

TABLE VI  
ABLATION EXPERIMENTS OF DIFFERENT COMPONENTS ON THE FOGGYCULANE DATASET.

Model	GFFM	KFFM	LEEM	F1-score	Gflops(G)
Baseline				77.85	13.77
	✓			78.26	11.94
	✓	✓		78.52	11.97
<b>Ours</b>	✓	✓	✓	<b>78.66↑</b>	12.01

FoggyCULane. Finally, the LEEM module improves edge detection, increasing the F1-score by 0.28 on FoggyLane and 0.14 on FoggyCULane.

#### F. Model deployment

To further evaluate the performance of our algorithm in real-world scenarios, in addition to experiments on existing datasets, we also deployed and tested the model on the vehicle. Specifically, we implemented an edge computing system on the vehicle, as illustrated in the Fig. 12. This system comprises the NVIDIA Jetson AGX Orin edge computing device, a monitor, a camera, and a power supply unit. The results of the evaluation demonstrate that our approach can operate in real-time with high accuracy on the vehicle's edge computing platform, despite the constraints on computational resources.

## VI. CONCLUSION

This study focuses on lane detection in foggy conditions, aiming to address the range of challenges posed by foggy

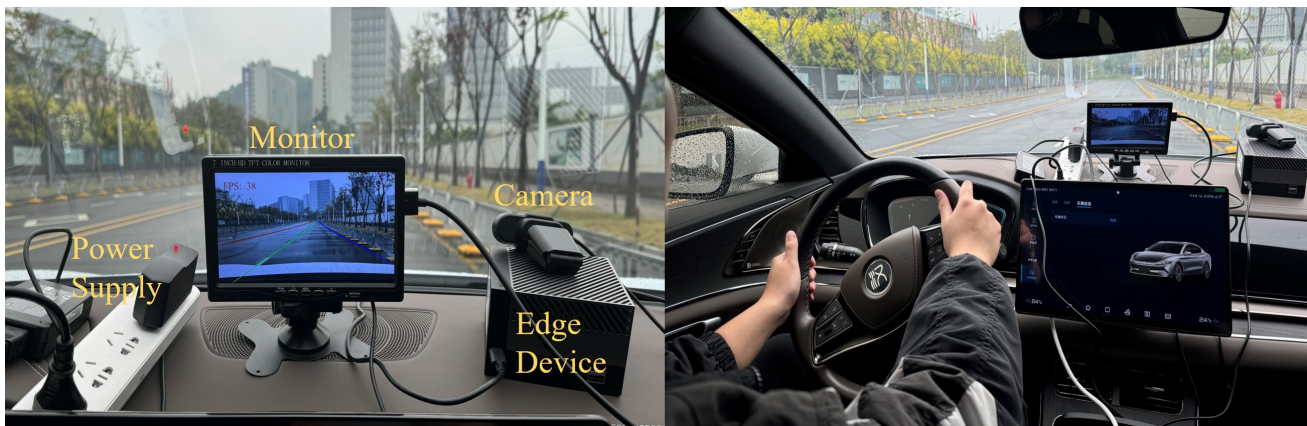


Fig. 12. A edge computing system built with NVIDIA Jetson AGX Orin. After experimental validation, it has been demonstrated that our method can run accurately on the vehicle's edge computing platform with limited computational resources, achieving a performance of 38.4 FPS.

environments, which is crucial for ensuring driving safety in fog and enhancing Advanced Driver Assistance System (ADAS) capabilities. To address the current lack of publicly available datasets for lane detection in foggy conditions, we constructed a real-world foggy lane dataset, FoggyLane, and synthesized two additional foggy datasets, FoggyCULane and FoggyTusimple, based on the popular CULane and Tusimple datasets.

In response to the challenges of lane detection in foggy scenarios, we propose an end-to-end fog-enhanced lane detection method. First, this method incorporates a Global Feature Fusion Module in the backbone network to address the absence of global spatial information in foggy scenes. Second, we employ a dynamic convolution-based detection head for instance-sensitive lane segmentation, integrating a Kernel Feature Fusion Module within the detection head to automatically capture associations between lane instances. Additionally, a Low-Level Edge Enhancement Module was added to increase the network's focus on edge information, mitigating the loss of edge details and improving lane detection accuracy under foggy conditions.

Comparative experiments on the FoggyLane, FoggyCULane, and FoggyTusimple datasets with other advanced lane detection methods demonstrate that our approach achieves superior performance in both clear and foggy conditions, significantly improving lane detection accuracy. Furthermore, with TensorRT acceleration, our method achieves an inference speed of 38.4 FPS on the NVIDIA Jetson AGX Orin, further validating its practical applicability in real-world scenarios.

#### ACKNOWLEDGMENTS

This project is jointly supported by National Natural Science Foundation of China (Nos. 52172350, W2421069 and 51775565), the Guangdong Basic and Applied Research Foundation (No. 2022B1515120072), the Guangzhou Science and Technology Plan Project (No. 2024B01W0079), the Nansha Key RD Program (No. 2022ZD014), the Science and Technology Planning Project of Guangdong Province (No. 2023B1212060029). **We would like to release our source code and dataset.**

#### REFERENCES

- [1] J. Bi, Y. Song, Y. Jiang, L. Sun, X. Wang, Z. Liu, J. Xu, S. Quan, Z. Dai, and W. Yan, "Lane detection for autonomous driving: Comprehensive reviews, current challenges, and future predictions," *IEEE Transactions on Intelligent Transportation Systems*, vol. 26, no. 5, pp. 5710–5746, 2025.
- [2] Pexels, <https://www.pexels.com/zh-cn/>, 2025.
- [3] J. Son, H. Yoo, S. Kim, and K. Sohn, "Real-time illumination invariant lane detection for lane departure warning system," *Expert Systems with Applications*, vol. 42, no. 4, pp. 1816–1824, 2015.
- [4] C. Hou, J. Hou, and C. Yu, "An efficient lane markings detection and tracking method based on vanishing point constraints," in *Chinese Control Conference (CCC)*. IEEE, 2016, pp. 6999–7004.
- [5] D. Neven, B. De Brabandere, S. Georgoulis, M. Proesmans, and L. Van Gool, "Towards end-to-end lane detection: an instance segmentation approach," in *2018 IEEE Intelligent Vehicles Symposium (IV)*. IEEE, 2018, pp. 286–291.
- [6] H. Abualsaud, S. Liu, D. B. Lu, K. Situ, A. Rangesh, and M. M. Trivedi, "Laneaf: Robust multi-lane detection with affinity fields," *IEEE Robotics and Automation Letters*, vol. 6, no. 4, pp. 7477–7484, 2021.
- [7] F. Yu, D. Wang, E. Shelhamer, and T. Darrell, "Deep layer aggregation," in *Proceedings of the IEEE Conference on Computer Vision and Pattern Recognition*, 2018, pp. 2403–2412.
- [8] X. Pan, J. Shi, P. Luo, X. Wang, and X. Tang, "Spatial as deep: Spatial cnn for traffic scene understanding," in *Proceedings of the AAAI Conference on Artificial Intelligence*, vol. 32, no. 1, 2018.
- [9] J. Shi, J. Zhao, D. Wang, and H. Tang, "Lane detection by variational auto-encoder with normalizing flow for autonomous driving," *IEEE Transactions on Intelligent Transportation Systems*, vol. 25, no. 12, pp. 21 757–21 768, 2024.
- [10] Y. Wen, Y. Yin, and H. Ran, "Flipnet: An attention-enhanced hierarchical feature flip fusion network for lane detection," *IEEE Transactions on Intelligent Transportation Systems*, vol. 25, no. 8, pp. 8741–8750, 2024.
- [11] Z. Qin, H. Wang, and X. Li, "Ultra fast structure-aware deep lane detection," in *European Conference on Computer Vision*. Springer, 2020, pp. 276–291.
- [12] J. Redmon, "You only look once: Unified, real-time object detection," in *Proceedings of the IEEE Conference on Computer Vision and Pattern Recognition*, 2016, pp. 779–788.
- [13] A. Farhadi and J. Redmon, "Yolov3: An incremental improvement," *arXiv preprint arXiv:1804.02767*, pp. 1–6, 2018.
- [14] S. Ren, K. He, R. Girshick, and J. Sun, "Faster r-cnn: Towards real-time object detection with region proposal networks," *IEEE Transactions on Pattern Analysis and Machine Intelligence*, vol. 39, no. 6, pp. 1137–1149, 2016.
- [15] W. Liu, D. Anguelov, D. Erhan, C. Szegedy, S. Reed, C.-Y. Fu, and A. C. Berg, "Ssd: Single shot multibox detector," in *European Conference on Computer Vision*. Springer, 2016, pp. 21–37.
- [16] Z. Chen, Q. Liu, and C. Lian, "Pointlanenet: Efficient end-to-end cnns for accurate real-time lane detection," in *2019 IEEE Intelligent Vehicles Symposium (IV)*. IEEE, 2019, pp. 2563–2568.

- [17] L. Tabelini, R. Berriel, T. M. Paixao, C. Badue, A. F. De Souza, and T. Oliveira-Santos, "Keep your eyes on the lane: Real-time attention-guided lane detection," in *Proceedings of the IEEE/CVF Conference on Computer Vision and Pattern Recognition*, 2021, pp. 294–302.
- [18] T. Zheng, Y. Huang, Y. Liu, W. Tang, Z. Yang, D. Cai, and X. He, "Clnet: Cross layer refinement network for lane detection," in *Proceedings of the IEEE/CVF Conference on Computer Vision and Pattern Recognition*, 2022, pp. 898–907.
- [19] H. Ran, Y. Yin, F. Huang, and X. Bao, "Flamnet: A flexible line anchor mechanism network for lane detection," *IEEE Transactions on Intelligent Transportation Systems*, vol. 24, pp. 12 767–12 778, 2023.
- [20] B. Liu and Q. Ling, "Sparse laneformer: End-to-end lane detection with sparse proposals and interactions," *IEEE Transactions on Intelligent Transportation Systems*, pp. 1–14, 2025.
- [21] S. Wang, J. Liu, X. Cao, Z. Song, and K. Sun, "Polar r-cnn: End-to-end lane detection with fewer anchors," *IEEE Transactions on Intelligent Transportation Systems*, pp. 1–13, 2025.
- [22] B. Liu and Q. Ling, "Hyper-anchor based lane detection," *IEEE Transactions on Intelligent Transportation Systems*, vol. 25, no. 10, pp. 13 240–13 252, 2024.
- [23] Y. Li, C. Wang, Y. Wang, M. Ren, J. Niu, J. Zhao, and K. Du, "Lane detection on rainy nights based on memory and discretization mechanisms," *IEEE Transactions on Intelligent Transportation Systems*, pp. 1–13, 2025.
- [24] S.-C. Huang, T.-H. Le, and D.-W. Jaw, "Dsnet: Joint semantic learning for object detection in inclement weather conditions," *IEEE Transactions on Pattern Analysis and Machine Intelligence*, vol. 43, no. 8, pp. 2623–2633, 2020.
- [25] X. Nie, Z. Xu, W. Zhang, X. Dong, N. Liu, and Y. Chen, "Foggy lane dataset synthesized from monocular images for lane detection algorithms," *Sensors*, vol. 22, no. 14, p. 5210, 2022.
- [26] Y. Chen, W. Li, C. Sakaridis, D. Dai, and L. Van Gool, "Domain adaptive faster r-cnn for object detection in the wild," in *Proceedings of the IEEE Conference on Computer Vision and Pattern Recognition*, 2018, pp. 3339–3348.
- [27] S. Zhang, H. Tuo, J. Hu, and Z. Jing, "Domain adaptive yolo for one-stage cross-domain detection," in *Asian Conference on Machine Learning*. PMLR, 2021, pp. 785–797.
- [28] M. Hniewa and H. Radha, "Multiscale domain adaptive yolo for cross-domain object detection," in *Proceedings of the IEEE International Conference on Image Processing*, 2021, pp. 3323–3327.
- [29] J. Li, R. Xu, J. Ma, Q. Zou, J. Ma, and H. Yu, "Domain adaptive object detection for autonomous driving under foggy weather," in *Proceedings of the IEEE/CVF Winter Conference on Applications of Computer Vision*, 2023, pp. 612–622.
- [30] Tusimple, <https://github.com/TuSimple/tusimple-benchmark>, 2017.
- [31] T. Zheng, H. Fang, Y. Zhang, W. Tang, Z. Yang, H. Liu, and D. Cai, "Resa: Recurrent feature-shift aggregator for lane detection," in *Proceedings of the AAAI Conference on Artificial Intelligence*, vol. 35, no. 4, 2021, pp. 3547–3554.
- [32] J. Zhao, Z. Qiu, H. Hu, and S. Sun, "Hwlane: Hw-transformer for lane detection," *IEEE Transactions on Intelligent Transportation Systems*, vol. 25, no. 8, pp. 9321–9331, 2024.
- [33] L. Tabelini, R. Berriel, T. M. Paixao, C. Badue, A. F. De Souza, and T. Oliveira-Santos, "Polylanenet: Lane estimation via deep polynomial regression," in *Proceedings of the IEEE International Conference on Pattern Recognition*. IEEE, 2021, pp. 6150–6156.
- [34] R. Liu, Z. Yuan, T. Liu, and Z. Xiong, "End-to-end lane shape prediction with transformers," in *Proceedings of the IEEE/CVF Winter Conference on Applications of Computer Vision*, 2021, pp. 3694–3702.
- [35] X. Dai, J. Xie, G. Zhang, K. Chang, F. Chen, Z. Wang, and C. Tang, "Dbnet: A curve-based dynamic association framework for lane detection," *IEEE Transactions on Intelligent Vehicles*, 2024.
- [36] Q. Li, X. Yu, J. Chen, B.-G. He, W. Wang, D. B. Rawat, and Z. Lyu, "Pga-net: Polynomial global attention network with mean curvature loss for lane detection," *IEEE Transactions on Intelligent Transportation Systems*, vol. 25, no. 1, pp. 417–429, 2024.
- [37] X. Li, J. Li, X. Hu, and J. Yang, "Line-cnn: End-to-end traffic line detection with line proposal unit," *IEEE Transactions on Intelligent Transportation Systems*, vol. 21, no. 1, pp. 248–258, 2019.
- [38] S. Yoo, H. S. Lee, H. Myeong, S. Yun, H. Park, J. Cho, and D. H. Kim, "End-to-end lane marker detection via row-wise classification," in *Proceedings of the IEEE/CVF Conference on Computer Vision and Pattern Recognition Workshops*, 2020, pp. 1006–1007.
- [39] L. Liu, X. Chen, S. Zhu, and P. Tan, "Condlanenet: A top-to-down lane detection framework based on conditional convolution," in *Proceedings of the IEEE/CVF International Conference on Computer Vision*, 2021, pp. 3773–3782.
- [40] GoogleMaps, <https://www.google.com/maps>, Accessed: 2024.
- [41] K. Behrendt and R. Soussan, "Unsupervised labeled lane markers using maps," in *Proceedings of the IEEE/CVF International Conference on Computer Vision Workshops*, 2019, pp. 832–839.
- [42] YouTube, <https://www.youtube.com/>, Accessed: 2024.
- [43] M. Aly, "Real time detection of lane markers in urban streets," in *2008 IEEE Intelligent Vehicles Symposium (IV)*. IEEE, 2008, pp. 7–12.
- [44] X. Huang, X. Cheng, Q. Geng, B. Cao, D. Zhou, P. Wang, Y. Lin, and R. Yang, "The apollo-scape dataset for autonomous driving," in *Proceedings of the IEEE Conference on Computer Vision and Pattern Recognition Workshops*, 2018, pp. 954–960.
- [45] F. Yu, H. Chen, X. Wang, W. Xian, Y. Chen, F. Liu, V. Madhavan, and T. Darrell, "Bdd100k: A diverse driving dataset for heterogeneous multitask learning," in *Proceedings of the IEEE/CVF Conference on Computer Vision and Pattern Recognition*, 2020, pp. 2636–2645.
- [46] H. Xu, S. Wang, X. Cai, W. Zhang, X. Liang, and Z. Li, "Curvelane-nas: Unifying lane-sensitive architecture search and adaptive point blending," in *European Conference on Computer Vision*. Springer, 2020, pp. 689–704.
- [47] R. Zhang, J. Peng, W. Gou, Y. Ma, J. Chen, H. Hu, W. Li, G. Yin, and Z. Li, "A robust and real-time lane detection method in low-light scenarios to advanced driver assistance systems," *Expert Systems with Applications*, vol. 256, p. 124923, 2024.
- [48] J. Wang, K. Sun, T. Cheng, B. Jiang, C. Deng, Y. Zhao, D. Liu, Y. Mu, M. Tan, X. Wang, W. Liu, and B. Xiao, "Deep high-resolution representation learning for visual recognition," *IEEE Transactions on Pattern Analysis and Machine Intelligence*, vol. 43, no. 10, pp. 3349–3364, 2021.
- [49] R. Zhang, S. Yang, D. Lyu, Z. Wang, J. Chen, Y. Ren, B. Gao, and Z. Lv, "Agaset: A robust road ponding detection method for proactive traffic safety," *IEEE Transactions on Intelligent Transportation Systems*, vol. 26, no. 1, pp. 497–516, 2025.
- [50] J. Chen, N. Zhao, R. Zhang, L. Chen, K. Huang, and Z. Qiu, "Refined crack detection via lcsformer for autonomous road inspection vehicles," *IEEE Transactions on Intelligent Vehicles*, vol. 8, no. 3, pp. 2049–2061, 2023.
- [51] R. Zhang, J. Peng, W. Gou, Y. Ma, J. Chen, H. Hu, W. Li, G. Yin, and Z. Li, "A robust and real-time lane detection method in low-light scenarios to advanced driver assistance systems," *Expert Systems with Applications*, vol. 256, p. 124923, 2024.
- [52] Z. Liu, Y. Lin, Y. Cao, H. Hu, Y. Wei, Z. Zhang, S. Lin, and B. Guo, "Swin transformer: Hierarchical vision transformer using shifted windows," in *Proceedings of the IEEE/CVF International Conference on Computer Vision*, 2021, pp. 10012–10022.
- [53] Z. Liu, H. Hu, Y. Lin, Z. Yao, Z. Xie, Y. Wei, J. Ning, Y. Cao, Z. Zhang, L. Dong *et al.*, "Swin transformer v2: Scaling up capacity and resolution," in *Proceedings of the IEEE/CVF Conference on Computer Vision and Pattern Recognition*, 2022, pp. 12 009–12 019.
- [54] X. Dong, J. Bao, D. Chen, W. Zhang, N. Yu, L. Yuan, D. Chen, and B. Guo, "Cswin transformer: A general vision transformer backbone with cross-shaped windows," in *Proceedings of the IEEE/CVF Conference on Computer Vision and Pattern Recognition*, 2022, pp. 12 124–12 134.
- [55] Z. Tian, B. Zhang, H. Chen, and C. Shen, "Instance and panoptic segmentation using conditional convolutions," *IEEE Transactions on Pattern Analysis and Machine Intelligence*, vol. 45, no. 1, pp. 669–680, 2023.



**Ronghui Zhang** received a B.Sc. (Eng.) from the Department of Automation Science and Electrical Engineering, Hebei University, Baoding, China, in 2003, an M.S. degree in Vehicle Application Engineering from Jilin University, Changchun, China, in 2006, and a Ph.D. (Eng.) in Mechanical & Electrical Engineering from Changchun Institute of Optics, Fine Mechanics and Physics, the Chinese Academy of Sciences, Changchun, China, in 2009. After finishing his post-doctoral research work at INRIA, Paris, France, in February 2011, he is currently an Associate Professor with the Research Center of Intelligent Transportation Systems, School of intelligent systems engineering, Sun Yat-sen University, Shenzhen, 518107, Guangdong, P.R.China. His current research interests include computer vision, intelligent control and ITS.





**Yuhang Ma** received his B.S. degree in Automation at Huazhong University of Science and Technology in 2020. He is currently pursuing the master's degree in Electronic and Information Engineering at Sun Yat-sen University, Shenzhen, 518107, Guangdong, P.R.China. His current research interests include autonomous driving and computer vision.



**Tengfei Li** received his B.S. degree in Robot Engineering from Harbin Institute of Technology at Weihai in 2024. He is currently pursuing the M.S. degree with the School of Intelligent Systems Engineering, Sun Yat-sen University. His research interests include computer vision and autonomous driving.



**Ziyu Lin** is currently pursuing a B.Sc. degree in Traffic Engineering with the School of intelligent systems engineering, Sun Yat-sen University, Guangzhou, China. Her research interests include computer vision, deep learning, and autonomous driving technology, with a particular focus on exploring how these technologies can enhance the efficiency and safety of autonomous driving.



**Yueying Wu** received her B.S. degree in Internet of Things Engineering from Central South University, Changsha, China, in 2020, and an M.S. degree in Transportation Engineering from Sun Yat-sen University, Shenzhen, 518107, Guangdong, P.R.China, in 2023. Her current research interests include autonomous driving and vehicle-road collaboration, deep learning and computer vision.



Yat-sen University. His research interests include computer vision, machine learning, intelligent transportation systems, mobile computing and medical image processing.



**Lin Zhang** received his Ph.D. in Automotive Engineering from Jilin University in 2019. He is currently an Associate Professor at the School of Automotive Studies at Tongji University, where his research interests primarily focus on vehicle motion control, automated driving decision-making, planning, and evaluation technology.



**Jia Hu** works as a ZhongTe Distinguished Chair in Cooperative Automation in the College of Transportation Engineering at Tongji University. Before joining Tongji, he was a research associate at the Federal Highway Administration, USA (FHWA). He is an Associate Editor of the IEEE Transaction on Intelligent Transportation Systems, IEEE Transaction on Intelligent Vehicle, American Society of Civil Engineers Journal of Transportation Engineering, IEEE Open Journal in Intelligent Transportation Systems, an assistant editor of the Journal of Intelligent Transportation Systems, an advisory editorial board member for the Transportation Research Part C, an associate editor for IEEE Intelligent Vehicles Symposium since 2018, and an associate editor for IEEE Intelligent Transportation Systems Conference since 2019. Furthermore, he is a member of TRB (a division of the National Academies) Vehicle Highway Automation Committee, Freeway Operation Committee and Simulation subcommittee of Traffic Signal Systems Committee, and a member of CAV Impact Committee and Artificial Intelligence Committee of ASCE Transportation and Development Institute.



**Tony Z. Qiu** is a Professor in the Faculty of Engineering at University of Alberta, Canada Research Chair Professor in Cooperative Transportation Systems, and Director of Centre for Smart Transportation. His research interest includes traffic operation and control, traffic flow theory, and traffic model analytics. He has published more than 180 papers in international journals and academic conferences, and has 7 awarded patents and 5 pending application patents. Dr. Qiu is working as the Managing Director for the ACTIVE-AURORA test bed network, which is Canadian National Connected Vehicle Test Bed, and sponsored by Transport Canada, City of Edmonton, Alberta Transportation and other funding agencies, to identify leading-edge Connected Vehicle solutions through research and development. His theoretical research has informed and enriched his many practical contributions, which have been widely supported by private and public sectors. Dr. Tony Qiu received his PhD degree from University of Wisconsin-Madison, and worked as a Post-Doctoral Researcher in the California PATH Program at the University of California, Berkeley before joining University of Alberta. Dr. Tony Qiu has been awarded Minister's Award of Excellence in 2013, Faculty of Engineering Annual Research Award in 2015-2016, and ITS Canada Annual Innovation and R & D Award in 2016 and 2017.



**Konghui Guo** received the B.S. degree from the Jilin University of Technology, Changchun, China, in 1956. He is currently with the National Automobile Dynamic Simulation Laboratory, Jilin University, Changchun, China. Since 1994, he has been an Academician with the Chinese Academy of Engineering. His research interests include the modeling and simulation of vehicle dynamics, tire dynamics, vehicle handling, and stability. He won seven prizes of Progress in Science and Technology awarded by the Chinese Government and the National Automatic Industry Corporation, China.